Sub-Meter Accurate Pedestrian Indoor Navigation System with Dual ZUPT-Aided INS, Machine Learning-Aided LTE, and UWB Signals

Chi-Shih Jao, Ali A. Abdallah, Changwei Chen, Minwon Seo, Solmaz S. Kia, Zaher M. Kassas, and Andrei M. Shkel
University of California, Irvine

BIOGRAPHY

Chi-Shih Jao received the B.S. degree in electrical engineering from the National Tsing Hua University, Hsinchu, Taiwan, in 2015, and the M.S. degree in electrical engineering from the Pennsylvania State University, University Park, PA, USA, in 2018. He is currently pursuing the Ph.D. degree with the Microsystems Laboratory, Department of Mechanical and Aerospace Engineering, University of California at Irvine. His research interests include inertial navigation by sensor fusion approach and vision-based inertial navigation. He was a recipient of the Holmes Fellowship from 2019 to 2020.

Ali A. Abdallah is pursuing a Ph.D. in Electrical Engineering and Computer Science (EECS), University of California at Irvine and a member of the Autonomous Systems Perception, Intelligence, and Navigation (ASPIN) Laboratory. He was a recipient of the Best Student Paper Award from the 2020 IEEE/ION Position, Location, and Navigation Symposium (PLANS) and the Grand Prize from the 2020 IEEE Signal Processing Society video contest for beamforming research (5-MICC).

Changwei Chen is a Ph.D. student in Cooperative Systems Lab at the University of California, Irvine (UCI). He received his M.S. degree in Mechanical and Aerospace Engineering from UCI and B.S. degree from Wuhan University of Technology, China. His research interests include the Integrity monitoring algorithms for multi-sensor systems, cooperative navigation of multiple mobile agents, Kalman filtering and sensor fusion. He is a recipient of the 2021-2022 Holmes Fellowship.

Min-Won Seo is a Ph.D. student in Cooperative Systems Lab, Department of Mechanical and Aerospace Engineering, University of California, Irvine, CA. He was a research engineer at LIG Nex1 Co., Ltd (formerly known as LG Innotek), Gyeonggi-do, South Korea from Jan. 2015-July. 2020. His research interest is in integrated sensing, perception, cooperative navigation of multi-agent systems, and their implementation.

Solmaz S. Kia is an Associate Professor of Mechanical and Aerospace Engineering at the University of California, Irvine (UCI). She obtained her Ph.D. degree in Mechanical and Aerospace Engineering from UCI, in 2009, and her M.Sc. and B.Sc. in Aerospace Engineering from the Sharif University of Technology, Iran, in 2004 and 2001, respectively. She was a senior research engineer at SySense Inc., El Segundo, CA from Jun. 2009 to Sep. 2010. She held postdoctoral positions in the Department of Mechanical and Aerospace Engineering at the University of California San Diego and UCI. She was a recipient of the UC president's postdoctoral fellowship in 2012-2014, an NSF CAREER award in 2017, and the best IEEE Control Systems Magazine paper award in 2021. Dr. Kia is an associate editor for IEEE Sensors Letters, IEEE Open Journal of Control Systems, Automatica (journal of IFAC), and IEEE Transactions on Control of Network Systems. Her main research interests, in a broad sense, include distributed optimization/coordination/estimation, nonlinear control theory, and probabilistic robotics.

Zaher (Zak) M. Kassas is Professor at The Ohio State University (OSU) and Director of the Autonomous Systems Perception, Intelligence, and Navigation (ASPIN) Laboratory. He is also Director of the U.S. Department of Transportation Center: CARMEN (Center for Automated Vehicle Research with Multimodal AssurEd Navigation), focusing on navigation resiliency and security of highly automated transportation systems. Prior to joining OSU, he was an Associate Professor at the University of California, Irvine (UCI). He received a B.E. in Electrical Engineering from the Lebanese American University, an M.S. in Electrical and Computer Engineering from The Ohio State University, and an M.S.E. in Aerospace Engineering and a Ph.D. in Electrical and Computer Engineering from The University of Texas at Austin. He is a recipient of the 2018 National Science Foundation (NSF) CAREER award, 2019 Office of Naval Research (ONR) Young Investigator Program (YIP) award, 2022 Air Force Office of Scientific Research (AFOSR) YIP award, 2018 IEEE Walter Fried Award, 2018 Institute of Navigation (ION) Samuel Burka Award, and 2019 ION Col. Thomas Thurlow Award. He is a Senior Editor of the IEEE Transactions on Intelligent Vehicles and an Associate Editor of the IEEE Transactions on Aerospace and Electronic Systems and the IEEE Transactions on Intelligent Transportation Systems. His research interests include cyber-physical systems, navigation systems, autonomous vehicles, and intelligent transportation systems.

Andrei M. Shkel received the diploma degree (Hons.) in mechanics and mathematics from Lomonosov's Moscow State University, Moscow, Russia, in 1991, and the Ph.D. degree in mechanical engineering from the University of Wisconsin–Madison,

Madison, WI, USA, in 1997. In 2000, he joined the Faculty of the University of California, Irvine, CA, USA, where he is currently a Professor with the Department of Mechanical and Aerospace Engineering. He has served as a Program Manager for the Microsystems Technology Office, Defense Advanced Research Projects Agency (DARPA), Arlington, VA, USA, from 2009 to 2013. His professional interests, reflected in over 300 publications and 3 books, include solid-state sensors and actuators, micro-electromechanical systems-based neuroprosthetics, sensor-based intelligence, and control theory. He holds over 42 issued patents. His current research interests include the design, manufacturing, and advanced control of high-precision micromachined gyroscopes and self-contained inertial navigation systems. He was a recipient of the 2002 George E. Brown, Jr., Award, the 2005 NSF CAREER Award, the 2006 UCI HSSoE Best Faculty Research Award, the 2009 IEEE Sensors Council Technical Achievement Award, and the 2020 UCI HSSoE Innovator of the Year Award. In 2013, he received the Office of the Secretary of Defense Medal for Exceptional Public Service. He has also served on a number of editorial boards, most recently, as an Editor for the IEEE/ASME JOURNAL OF MICROELECTROMECHANICAL SYSTEMS, the Journal of Gyroscopy and Navigation, and the Founding Chair for the IEEE International Symposium on Inertial Sensors and Systems (INERTIAL). He is the IEEE Fellow and the Past President of the IEEE Sensors Council (2020-2021). In 2021, he was elected to National Academy of Inventors (NAI) Fellow status.

ABSTRACT

Developing a universal pedestrian navigation framework that operates through extreme environmental conditions is essential. Such a navigation framework can enable Location-Based Services (LBS) in many applications, and one application in high demand of accurate and reliable positioning solutions is firefighter localization, primarily for navigating in indoor environments where signals of Global Navigation Satellite Systems (GNSS) might degrade or fail, visibility is poor, and infrastructure dedicated to navigation is often not accessible. Jao et al. (2022a) reported a Pedestrian Indoor Navigation system integrating Deterministic, Opportunistic, and Cooperative localization approaches (PINDOC). The deterministic localization is a Zero-velocity-UPdaTe (ZUPT)-aided Inertial Navigation System (INS) enhanced with self-contained aiding approaches, including altimeter measurements and foot-to-foot ranging measurements. The opportunistic approach uses pseudorange measurements extracted from cellular Long-Term Evolution (LTE) towers and implements a Deep Neural Network (DNN)-based Synthetic Aperture Navigation (SAN) to spatially mitigate multipath. This approach operates in a base/rover framework, where a GNSS receiver and a "base" LTE receiver, both installed stationary in an outdoor environment, are used to estimate clock bias drifts of LTE towers, and the estimated clock biases are transmitted to "rover" LTE receivers equipped on agents navigating in indoor environments. The cooperative localization approach uses UWBs for inter-agent range measurements and differentiates Line-Of-Sight (LOS) and NLOS components using a power-metric-based detector. In this paper, we experimentally investigate the navigation performance of the PINDOC system. Two experiments were conducted. The first experiment involved three agents, with one agent traversing in an indoor environment a trajectory of 600 meters in 14 minutes, during which the other two agents remained stationary. The traversed trajectory included terrains of flat surfaces, stairs, ramps, and elevators. The PINDOC system achieved a position Root-Mean-Squared Error (RMSE), maximum error, and loop-closure error of 0.93 m, 2.23 m, and 1.28 m over the 600-meter trajectory, respectively. In the second experiment, all three agents traveled in the indoor environment for 12.5 minutes, and the navigation solutions estimated by the PINDOC system showed loop-closure errors of 0.35 m, 0.82, and 1.15 m for the three agents. In all cases, access to signals of opportunity and cooperative exchange of information between agents were available less than 20% of time for duration of the experiments.

I. INTRODUCTION

Developing an accurate and reliable universal pedestrian navigation framework can enable Location-Based Services (LBS) in multiple different applications, including contact tracing (Kleinman and Merkel, 2020), warehouse inventory management (Tejesh and Neeraja, 2018), shopping (Renaudin et al., 2019), gaming (Sevrin et al., 2015), and firefighter tracking (Ferreira et al., 2017). This universal navigation framework needs to maintain low positioning errors for a long period of time and cover various challenging scenarios, such as indoor environments, urban canyons, forest canopies, and underground caves. These scenarios often come with conditions that signals of Global Navigation Satellite Systems (GNSS) are degraded or unavailable, visibility is poor due to smoke or low light intensity, and infrastructures dedicated to navigation are not accessible. These strict requirements eliminate the possibility of independently utilizing many existing positioning technologies, including cameras (Lemaire et al., 2007), Light Detection and Ranging (LiDAR) (Kumar et al., 2017), Radio-Frequency (RF) systems based on Bluetooth (Zhuang et al., 2016), Wi-Fi (Shu et al., 2015), cellular Long-Term Evolution (LTE) (Shamaei and Kassas, 2018), or Ultra-WideBand (UWB) (Ruiz and Granja, 2017), and Inertial Navigation Systems (INS) (Titterton and Weston, 2004). In order to operate through extreme conditions, a potential pedestrian navigation solution is to integrate positioning technologies that have complementary localization properties. INS is a preferable option to be integrated into such a pedestrian system as it operates in a self-contained manner, requires no installation time, and provides consistently available measurements. Despite these attractive features, without an aiding source, the errors in an INS accumulate over time, causing the navigation solution to eventually drift unboundedly (Jao et al., 2020a).

Zero-velocity UPdaTe (ZUPT) algorithm has been used in a pedestrian INS as an effective aiding approach to significantly enhance the performance of a strapdown INS (Foxlin, 2005). The ZUPT algorithm uses Inertial Measurement Units (IMUs) mounted on a person's foot and makes an assumption that the velocities of a person's foot during walking are nearly equal to zero during the stance phase of a gait cycle (Nilsson et al., 2014). With this assumption, the algorithm periodically resets the residual velocities in every step, effectively reducing localization errors caused by noise and stochastic time-varying biases of IMUs in an INS (Jao and Shkel, 2021b). The ZUPT-aided INS is conventionally implemented in an Extended Kalman Filter (EKF) framework, where pseudo measurements of zero-velocity are feedback to the system when stance phases are detected (Jao and Shkel, 2021a). It has been mathematically shown that this implementation has bounded error growth not only for the velocity states along the three axes but also for the two orientation states along pitch and roll directions (Nilsson et al., 2013). The ZUPT-aided INS implemented in the EKF has been theoretically predicted and experimentally demonstrated to achieve an error of less than 1% of the traveling distance with an industrial-grade IMU (Wang et al., 2018b, 2020, 2021).

The conventional ZUPT-aided INS, however, has unbounded error growth for the position states along the three axes and the yaw angle state (Nilsson et al., 2012). Moreover, the algorithm has been identified with multiple error sources, including 1) noise characteristics of deployed IMUs, 2) performance of stance phase detection, 3) insufficient sensor Full-Scale Range (FSR) and bandwidth, and 4) unmodeled error that results from a violation of the assumption that the foot is completely stationary during the stance phase of a gait cycle (Wahlström and Skog, 2020). These errors led the ZUPT-aided INS to have long-term position drifts. To further improve navigation accuracy of the ZUPT-aided INS, sensor fusion solutions based on different non-inertial sensing modalities have been popular approaches (Jao et al., 2020c). In this paper, we grouped the sensor fusion enhancement techniques into deterministic, opportunistic, and cooperative localization approaches.

The *deterministic* approach is referred to as the ZUPT-aided INS augmented by self-contained aiding approaches, which use sensors that are collocated with a foot-mounted IMU (Shkel and Wang, 2021). The self-contained approaches include different implementations, such as barometric altimeters (Jao et al., 2020a) or hybrid ultrasonic/barometric altimeters (Jao et al., 2020b) for providing vertical displacement compensation; magnetometers (Wang et al., 2018a), foot-to-foot ultrasonic sensors (Laverne et al., 2011; Wang et al., 2019), and foot-to-foot cameras (Jao et al., 2020c) for increasing observability in the yaw angle estimation; or downward-facing ultrasonic sensors (Jao et al., 2020d, 2021), Dynamic Vision Sensors (DVS) (Jao et al., 2020e), pressure sensors (Ma et al., 2018), and permanent magnets (Norrdine et al., 2016) for increasing the stance phase detection performance. The deterministic localization approach has been demonstrated to improve navigation accuracy, as compared to a standalone ZUPT-aided INS (Wang et al., 2021). Nevertheless, absolute horizontal position uncertainties of the former systems propagate unboundedly and can eventually exceed desired localization accuracy in long-term pedestrian navigation. To improve localization accuracy of the deterministic localization, infrastructure-free solutions using opportunistic exteroceptive external aiding signals have been explored. These aiding signals can be implemented as Cooperative Localization (CL) (Zhu and Kia, 2019b; Minetto and Dovis, 2019; Zhu and Kia, 2021) or opportunistic localization (Ikhtiari, 2019; Abdallah et al., 2022; Souli et al., 2021b; Whiton et al., 2022) or a combination thereof (Souli et al., 2021a).

In the *cooperative* approach, a group of communicating agents uses inter-agent relative measurements as feedback to improve the localization accuracy of their local filter, e.g., Pedestrian INS (Zhu and Kia, 2018). CL in pedestrian navigation can be implemented based on inter-agent range measurements obtained using different mechanisms, including computer vision or wireless radio signals (de Ponte Müller, 2017). Among these implementations, range measurements collected from UWB modules have attracted significant attention in indoor navigation for the sensor's high time resolution, wide bandwidth, and capability to work under Non-Line-Of-Sight (NLOS) conditions (Zhu and Kia, 2021). On the other hand, in an *opportunistic* localization framework, cellular towers are treated as beacons, and positioning can be achieved by trilaterating pseudorange measurements based on cellular signals (Kassas, 2021). Cellular signals possess several desirable characteristics for indoor localization (Kassas et al., 2017a; Strandjord et al., 2021; Yang et al., 2022; Pan et al., 2022): abundance, geometric diversity, high bandwidth, high carrier-to-noise ratio (C/N_0) indoors, and the fact that some of their downlink signals are free to use (Abdallah et al., 2021). Cooperative and signal-based localization approaches have been demonstrated to provide relative and absolute position compensations to deterministic approaches (Kassas et al., 2017b; Maaref and Kassas, 2022; Morales et al., 2022). However, to the authors' knowledge, not much effort has been put into developing a navigation solution integrating the three localization approaches (deterministic, cooperative, and opportunistic) for indoor navigation.

We have previously developed a Pedestrian Indoor Navigation system integrating Deterministic, Opportunistic, and Cooperative functionalities (PINDOC) for navigation of multiple agents and reported the algorithmic and the hardware framework as well as experimental results of the PINDOC system in Jao et al. (2022a). In this paper, we further investigated the navigation performance of the PINDOC by experimentally evaluating the navigation performance and repeatability of the system with multiple multi-agent indoor navigation experiments.

The rest of the paper is organized as follows: Section II presents the algorithm framework that combines the deterministic, opportunistic, and cooperative localization approaches. Section III discusses a pedestrian navigation testbed capable of collecting sensor measurements used in the three localization approaches. Section IV presents the experimental results. Section V concludes the paper with a highlight of experimental performance of the PINDOC system.

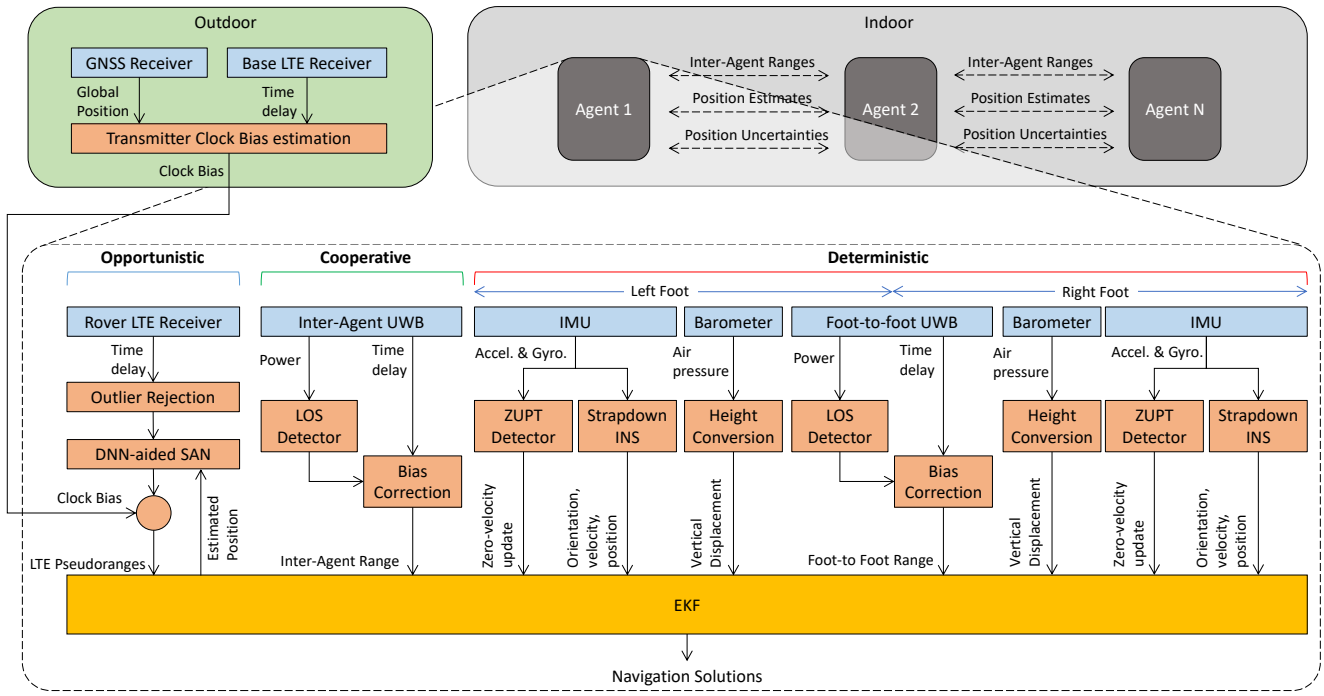

Figure 1: A block diagram illustrating the PINDOC system. The system integrates deterministic, opportunistic, and cooperative localization approaches. The deterministic approach uses a ZUPT-aided INS augmented with altimeter measurements and foot-to-foot ranging measurements. The opportunistic approach provides global position compensation based on machine-learning-aided LTE psuedoranges. The cooperative localization approach is achieved based on inter-agent range measurements.

II. ALGORITHM DESIGN

The PINDOC system used in this paper integrates deterministic, opportunistic, and cooperative localization components. The deterministic component implements a ZUPT-aided INS augmented with a barometric altimeter and foot-to-foot range enhancement. The opportunistic approach uses Deep Neural Network (DNN)-aided Synthetic Aperture Navigation (SAN) enhanced Long-Term Evolution (LTE) pseudoranges. The cooperative localization is based on inter-agent UWB range measurements. Figure 1 presents a block diagram illustrating the PINDOC system. The system is realized in an EKF framework, where the prediction step propagates navigation states with a strapdown INS and an LTE clock drift model, and the update step compensates the states with measurements of vertical positions, foot-to-foot distances, inter-agent distances, and absolute positions. In this section, we describe the EKF states, the EKF prediction step, and the EKF update step.

1. EKF States

The EKF estimates the state vector $\mathbf{x}(k)$ for a group of N agents, expressed as:

$$\mathbf{x}(k) = [\mathbf{x}_{\mathrm{A}_1}^\top(k), \mathbf{x}_{\mathrm{A}_2}^\top(k), \ldots, \mathbf{x}_{\mathrm{A}_N}^\top(k), \mathbf{x}_{\mathrm{LTE}_1}^\top(k), \mathbf{x}_{\mathrm{LTE}_2}^\top(k), \ldots, \mathbf{x}_{\mathrm{LTE}_N}^\top(k)]^\top,$$

where A_i denotes agent i in the group, and $\mathbf{x}_{\mathrm{A}_i}(k)$ and $\mathbf{x}_{\mathrm{LTE}_i}(k)$ are the states associated with agent i, described as

$$\mathbf{x}_{\mathrm{A}_i}(k) = [\mathbf{q}_{\mathrm{A}_i^l}^\top(k), \mathbf{v}_{\mathrm{A}_i^l}^\top(k), \mathbf{p}_{\mathrm{A}_i^l}^\top(k), \mathbf{b}_{a,\mathrm{A}_i^l}^\top(k), \mathbf{b}_{g,\mathrm{A}_i^l}^\top(k), \mathbf{q}_{\mathrm{A}_i^r}^\top(k), \mathbf{v}_{\mathrm{A}_i^r}^\top(k), \mathbf{p}_{\mathrm{A}_i^r}^\top(k), \mathbf{b}_{a,\mathrm{A}_i^r}^\top(k), \mathbf{b}_{g,\mathrm{A}_i^r}^\top(k)]^\top \in \mathbb{R}^{30\times 1},$$
$$\mathbf{x}_{\mathrm{LTE}_i}(k) = [c\delta t_{\mathrm{rx}_i}(k), c\dot{\delta} t_{\mathrm{rx}_i}(k)]^\top \in \mathbb{R}^{2\times 1},$$

where $\mathbf{q}_{\mathrm{A}_i^l}(k), \mathbf{v}_{\mathrm{A}_i^l}(k), \mathbf{p}_{\mathrm{A}_i^l}(k), \mathbf{b}_{a,\mathrm{A}_i^l}(k)$, and $\mathbf{b}_{g,\mathrm{A}_i^l}(k)$ represent states of the left foot of agent i, including orientations, velocities, positions in the navigation frame, and accelerometer and gyroscope biases in the sensor body frame. $\mathbf{q}_{\mathrm{A}_i^r}(k), \mathbf{v}_{\mathrm{A}_i^r}(k), \mathbf{p}_{\mathrm{A}_i^r}(k), \mathbf{b}_{a,\mathrm{A}_i^r}(k)$, and $\mathbf{b}_{g,\mathrm{A}_i^r}(k)$ are the corresponded states of the right foot agent i. $c\delta t_{\mathrm{rx}_i}(k)$ and $c\dot{\delta} t_{\mathrm{rx}_i}(k)$ indicate the speed of light, c, multiplied by estimated clock bias and drift of an LTE receiver mounted on agent i. This expression of $\mathbf{x}_{\mathrm{LTE}_i}(k)$ has a unit of meter, which is beneficial for numerical calculations, as compared to directly using clock bias and drift.

2. EKF Prediction Step

a) Strapdown Inertial Navigation Systems

In the prediction step of the EKF, propagation of the states $\mathbf{x}_{\mathrm{A}_i}(k)$ is implemented by inputting the IMU measurements on each foot to the strapdown inertial navigation systems (Titterton and Weston, 2004). The linearized state transition matrix corresponding to strapdown INS, denoted as $\mathbf{F}_{\text{INS}}(k)$, is expressed as follows:

$$\mathbf{F}_{\text{INS}}(k) = e^{\mathbf{A}_{\text{INS}}(t_k)dt},$$

where dt is the sampling rate of the system and

$$\mathbf{A}_{\text{INS}}(t) = \begin{bmatrix} \mathbf{A}_{\mathrm{A}_1}(t) & \mathbf{0}_{30\times30} & \dots & \mathbf{0}_{30\times30} \\ \mathbf{0}_{30\times30} & \mathbf{A}_{\mathrm{A}_2}(t) & & \vdots \\ \vdots & & \ddots & \mathbf{0}_{30\times30} \\ \mathbf{0}_{30\times30} & \dots & \mathbf{0}_{30\times30} & \mathbf{A}_{\mathrm{A}_N}(t) \end{bmatrix},$$

with

$$\mathbf{A}_{\mathrm{A}_i}(t) = \begin{bmatrix} \mathbf{A}_{\mathrm{A}_i^l}(t) & \mathbf{0}_{15\times15} \\ \mathbf{0}_{15\times15} & \mathbf{A}_{\mathrm{A}_i^r}(t) \end{bmatrix}, \text{ and } \mathbf{A}_{\mathrm{A}_i^l}(t) = \begin{bmatrix} \mathbf{0}_{3\times3} & \mathbf{0}_{3\times3} & \mathbf{0}_{3\times3} & -\mathrm{C}(\mathbf{q}_{\mathrm{A}_i^l}(k)) & \mathbf{0}_{3\times3} \\ [\overrightarrow{f_l}^n\times] & \mathbf{0}_{3\times3} & \mathbf{0}_{3\times3} & \mathbf{0}_{3\times3} & \mathrm{C}(\mathbf{q}_{\mathrm{A}_i^l}(k)) \\ \mathbf{0}_{3\times3} & \mathbf{I}_{3\times3} & \mathbf{0}_{3\times3} & \mathbf{0}_{3\times3} & \mathbf{0}_{3\times3} \\ \mathbf{0}_{3\times3} & \mathbf{0}_{3\times3} & \mathbf{0}_{3\times3} & \mathbf{0}_{3\times3} & \mathbf{0}_{3\times3} \\ \mathbf{0}_{3\times3} & \mathbf{0}_{3\times3} & \mathbf{0}_{3\times3} & \mathbf{0}_{3\times3} & \mathbf{0}_{3\times3} \end{bmatrix}.$$

Here, $[\overrightarrow{f_l}^n\times]$ is the skew-symmetric cross-product-operator of the accelerometer outputs of the left IMU, expressed in the navigation frame. $\mathrm{C}(\mathbf{q})$ is the Directional Cosine Matrix (DCM) corresponding to the quaternion vector $\mathbf{q}$. $\mathbf{0}_{n\times m}$ indicates a zero matrix having n number of rows and m number of columns. $\mathbf{A}_{\mathrm{A}_i^r}(t)$ is constructed in the same manner as $\mathbf{A}_{\mathrm{A}_i^l}(t)$ except that the states corresponding to the right foot are used.

The process noise matrix corresponding to strapdown INS, denoted as $\mathbf{Q}_{\text{INS}}(k)$, is expressed as

$$\mathbf{Q}_{\text{INS}}(k) = \begin{bmatrix} \mathbf{Q}_{\mathrm{A}_1}(k) & \mathbf{0}_{30\times30} & \dots & \mathbf{0}_{30\times30} \\ \mathbf{0}_{30\times30} & \mathbf{Q}_{\mathrm{A}_2}(k) & & \vdots \\ \vdots & & \ddots & \mathbf{0}_{30\times30} \\ \mathbf{0}_{30\times30} & \dots & \mathbf{0}_{30\times30} & \mathbf{Q}_{\mathrm{A}_N}(k) \end{bmatrix}, \mathbf{Q}_{\mathrm{A}_i}(k) = \begin{bmatrix} \mathbf{Q}_{\mathrm{A}_i^l}(k) & \mathbf{0}_{15\times15} \\ \mathbf{0}_{15\times15} & \mathbf{Q}_{\mathrm{A}_i^r}(k) \end{bmatrix},$$

with

$$\mathbf{Q}_{\mathrm{A}_i^l}(k) = \begin{bmatrix} \sigma^2_{\text{ARW}}\mathbf{I}_{3\times3} & \mathbf{0}_{3\times3} & \mathbf{0}_{3\times3} & \mathbf{0}_{3\times3} & \mathbf{0}_{3\times3} \\ \mathbf{0}_{3\times3} & \sigma^2_{\text{VRW}}\mathbf{I}_{3\times3} & \mathbf{0}_{3\times3} & \mathbf{0}_{3\times3} & \mathbf{0}_{3\times3} \\ \mathbf{0}_{3\times3} & \mathbf{I}_{3\times3} & \mathbf{0}_{3\times3} & \mathbf{0}_{3\times3} & \mathbf{0}_{3\times3} \\ \mathbf{0}_{3\times3} & \mathbf{0}_{3\times3} & \mathbf{0}_{3\times3} & \sigma^2_{\text{AcRW}}\mathbf{I}_{3\times3} & \mathbf{0}_{3\times3} \\ \mathbf{0}_{3\times3} & \mathbf{0}_{3\times3} & \mathbf{0}_{3\times3} & \mathbf{0}_{3\times3} & \sigma^2_{\text{RRW}}\mathbf{I}_{3\times3} \end{bmatrix}.$$

Here, $\mathbf{I}_{n\times n}$ is the identity matrix having n number of rows and columns. $\sigma^2_{\text{ARW}_i}$, $\sigma^2_{\text{VRW}_i}$, $\sigma^2_{\text{RRW}_i}$, and $\sigma^2_{\text{AcRW}_i}$ are the Angle Random Walk of the gyroscopes, the Velocity Random Walk of the accelerometers, the Rate Angle Walk of the gyroscopes, and the Acceleration Random Walk of the accelerometers of the IMU mounted on the left shoe of agent i. In this paper, we set $\mathbf{Q}_{\mathrm{A}_i^r}(k) = \mathbf{Q}_{\mathrm{A}_i^l}(k)$ based on an assumption that two IMUs, each mounted on the same agent's left and right feet, have similar noise characteristics.

b) LTE Clock Drift Propagation

The EKF prediction step propagates the state $\mathbf{x}_{\text{LTE}_i}(k)$ with following state transition matrix $\mathbf{F}_{\text{LTE}_i}(k)$ and process noise covariance $\mathbf{Q}_{\text{LTE}_i}(k)$

$$\mathbf{F}_{\text{LTE}_i}(k) = \begin{bmatrix} 1 & dt \\ 0 & 1 \end{bmatrix}, \mathbf{Q}_{\text{LTE}_i}(k) = c^2 \begin{bmatrix} \sigma_{\delta t_{rx_i}} dt + \sigma_{\dot{\delta} t_{rx_i}} \frac{dt^3}{3} & \sigma_{\dot{\delta} t_{rx_i}} \frac{dt^2}{2} \\ \sigma_{\dot{\delta} t_{rx_i}} \frac{dt^2}{2} & \sigma_{\dot{\delta} t_{rx_i}} dt, \end{bmatrix}$$

where $\sigma_{\delta t_{rx_i}}$ and $\sigma_{\dot{\delta t}_{rx_i}}$ are parameters associated with clock quality. Details regarding modeling of the clock bias and drift are documented in Abdallah and Kassas (2021).

3. EKF Update Step

a) Zero-Velocity Update Algorithm

When a stance phase is detected, the ZUPT algorithm is activated to compensate for the velocity state in the update step of the EKF. The compensation is done by feeding in pseudo-measurements of zero velocity along the three axes, which is denoted as $\mathbf{v}_{\text{ZUPT}}(k) = \mathbf{0}_{3\times 1}$. In this paper, the stance phase detection is achieved with the Stance Hypothesis Optimal dEtection (SHOE) detector (Skog et al., 2010), which determines a stance phase if

$$T(\mathbf{u}_n) = \frac{1}{N}\sum_{k\in\Omega_n}\left(\frac{1}{\sigma_\alpha^2}\parallel \mathbf{y}_k^\alpha - g\frac{\bar{\mathbf{y}}_k^\alpha}{\parallel \bar{\mathbf{y}}_k^\alpha \parallel}\parallel^2 + \frac{1}{\sigma_\omega^2}\parallel \mathbf{y}_k^\omega \parallel^2\right) < \gamma,$$

where $\mathbf{u}_n = \{\mathbf{y}_k\}_{k=n}^{k=N-1}$ with $\mathbf{y}_k = [\mathbf{y}_k^\alpha, \mathbf{y}_k^\omega]^\top$, $\mathbf{y}_k^\alpha$ is 3-axis accelerometer measurements at time k, $\mathbf{y}_k^\omega$ is 3-axis gyroscope measurements at time k, g is the gravitational constant, $\Omega_n = \{l \in \mathbb{N}, n \le l < N-1\}$ is a collection of the sensor measurement indexes at time n with a window of length N, and γ are user-defined thresholds.

For the states associated with the left and the right feet of agent i, the ZUPT measurement models, $\mathbf{z}_{\text{ZUPT}_i^l}(k)$ and $\mathbf{z}_{\text{ZUPT}_i^r}(k)$, measurement matrices, $\mathbf{H}_{\text{ZUPT}_i^l}(k)$ and $\mathbf{H}_{\text{ZUPT}_i^r}(k)$, and measurement covariance matrices, $\mathbf{R}_{\text{ZUPT}_i^l}(k)$ and $\mathbf{R}_{\text{ZUPT}_i^r}(k)$, are expressed as follows:

$$\mathbf{z}_{\text{ZUPT}_i^l}(k) = \mathbf{z}_{\text{ZUPT}_i^r}(k) = \mathbf{v}_{\text{ZUPT}}(k)$$

$$\mathbf{H}_{\text{ZUPT}_i^l}(k) = \begin{bmatrix} \mathbf{0}_{((i-1)\times 30+3)\times 3} \\ \mathbf{I}_{3\times 3} \\ \mathbf{0}_{(24+(N-i)\times 30+2N)\times 3} \end{bmatrix}^\top, \mathbf{H}_{\text{ZUPT}_i^r}(k) = \begin{bmatrix} \mathbf{0}_{((i-1)\times 30+18)\times 3} \\ \mathbf{I}_{3\times 3} \\ \mathbf{0}_{(9+(N-i)\times 30+2N)\times 3} \end{bmatrix}^\top$$

$$\mathbf{R}_{\text{ZUPT}_i^l}(k) = \mathbf{R}_{\text{ZUPT}_i^r}(k) = \sigma^2_{\text{ZUPT}_i}\mathbf{I}_{3\times 3},$$

where $\sigma^2_{\text{ZUPT}_i}$ is the noise variance of the zero-velocity measurement $\mathbf{v}_{\text{ZUPT}}$ for agent i.

b) Height Compensation

In a pedestrian navigation system based on foot-mounted IMUs, altitude measurements can be obtained from a barometer (Jao et al., 2020a) or, in a hybrid approach, using both barometer and ultrasonic sensors (Jao et al., 2020b). At time k, altimeters mounted on the left and the right shoes of agent i provide measurements of vertical displacements in the navigation frame, which are denoted as $d_{\perp_i^l}(k)$ and $d_{\perp_i^r}(k)$, respectively. The altimeter measurements are used in the update step of the EKF to bound error growth of estimated position along the vertical direction (Jao et al., 2020a). The measurement models corresponding to the altimeter on the left and right feet of agent i, $z_{\text{ALT}_i^l}(k)$ and $z_{\text{ALT}_i^r}(k)$, are described as follows:

$$z_{\text{ALT}_i^l}(k) = d_{\perp_i^l}(k), z_{\text{ALT}_i^r}(k) = d_{\perp_i^r}(k).$$

The associated measurement matrices are described as

$$\mathbf{H}_{\text{ALT}_i^l}(k) = \begin{bmatrix} \mathbf{0}_{1\times((i-1)\times 30+8)} \\ 1 \\ \mathbf{0}_{1\times(21+(N-i)\times 30+2N)} \end{bmatrix}^\top, \mathbf{H}_{\text{ALT}_i^r}(k) = \begin{bmatrix} \mathbf{0}_{1\times((i-1)\times 30+23)} \\ 1 \\ \mathbf{0}_{1\times(6+(N-i)\times 30+2N)} \end{bmatrix}^\top.$$

The measurement noise covariance matrices are described as

$$\mathbf{R}_{\text{ALT}_i^l}(k) = \mathbf{R}_{\text{ALT}_i^r}(k) = \sigma^2_{\text{ALT}_i},$$

where $\sigma^2_{\text{ALT}_i}$ is the noise variance of the altimeter measurements for agent i.

c) Inter-foot Ranging Enhancement

Distance measurements between the two feet of agent i, denoted as $r_{\text{F2F}_i}(k)$, can be obtained from various different sensing modalities, including ultrasonic sensors (Wang et al., 2019), foot-to-foot cameras (Jao et al., 2020c), electromagnetic systems

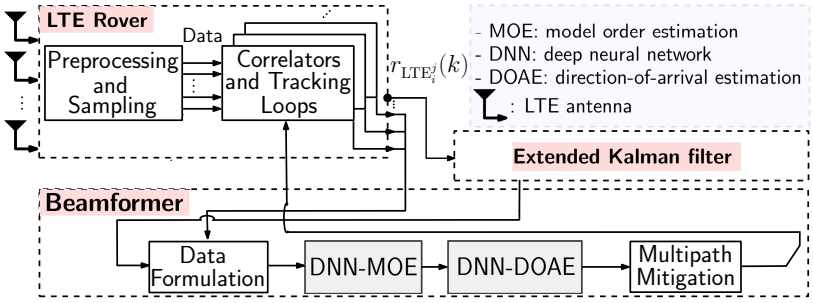

Figure 2: A block diagram depicting the LTE-DNN-SAN block diagram used in the proposed PINDOC framework shown in Figure 1

(Wang et al., 2020), and UWB (Zhu and Kia, 2020; Chen et al., 2022). In this paper, foot-to-foot ranging measurements are collected with a pair of UWB modules that are mounted on two different shoes. The UWB-based foot-to-foot range measurements are classified into LOS and NLOS by a power metric-based approach (Zhu and Kia, 2021). In this paper, only LOS UWB measurements are used. The range measurements are processed with bias correction. The processed foot-to-foot measurements are fused in the update step of the EKF to compensate for relative distances between the two feet (Laverne et al., 2011). The corresponding measurement model, $z_{\text{F2F}_i}(k)$, measurement matrix, $\mathbf{H}_{\text{F2F}_i}(k)$, and measurement noise covariance matrices, $\mathbf{R}_{\text{F2F}_i}(k)$, are described as follows:

$$z_{\text{F2F}_i}(k) = r_{\text{F2F}_i}(k),$$

$$\mathbf{H}_{\text{F2F}_i}(k) = \begin{bmatrix} \mathbf{0}_{((i-1)\times 30+6)\times 1} \\ \frac{\partial ||\mathbf{p}_{\text{A}_i^l}(k) - \mathbf{p}_{\text{A}_i^r}(k)||^\top}{\partial \mathbf{p}_{\text{A}_i^l}} \\ \mathbf{0}_{15\times 1} \\ \frac{\partial ||\mathbf{p}_{\text{A}_i^l(k)} - \mathbf{p}_{\text{A}_i^r}(k)||^\top}{\partial \mathbf{p}_{\text{A}_i^r(k)}} \\ \mathbf{0}_{(6+(N-i)\times 30+2N)\times 1} \end{bmatrix}^\top,$$

$$\mathbf{R}_{\text{F2F}_i}(k) = \sigma^2_{\text{F2F}_i},$$

where $\sigma^2_{\text{F2F}_i}$ is the noise variance of the foot-to-foot range measurements for agent i.

d) LTE Machine Learning-Aided SAN

In the opportunistic framework, cellular LTE signals are utilized to provide absolute positioning measurements. This is achieved by exploiting LTE downlink signals opportunistically in a base/rover LTE-DNN-SAN framework. In the opportunistic framework, a "base" LTE receiver is located outside the building and has access to GNSS signals. The base collects signals from multiple LTE towers (also known as eNodeBs) in the environment. The positions of the eNodeBs are pre-surveyed and assumed to be known (e.g., according to Morales and Kassas (2018)). The base receiver estimates the eNodeBs' clock biases and shares this information with the indoor receivers denoted by "rovers." Such setup ensures state observability (Kassas and Humphreys, 2014; Morales and Kassas, 2019). Each rover has a copy of the same LTE receiver used in the base unit. To compensate for multipath-induced biases that are known to significantly degrade the positioning accuracy (Wang and Morton, 2020; Dun et al., 2020; Xu and Rife, 2020; Wang et al., 2022), a DNN-based SAN correction block is applied, in which the pedestrian's motion is utilized to synthesize a geometrically-separated antenna array from time-separated snapshots. This allows for beamforming towards the LOS from the rover to the LTE eNodeB, while suppressing multipath components. This process requires obtaining the LOS steering vector, which is obtained by taking the nearest direction-of-arrival (DOA) estimate from the proposed DNN-DOA estimator to the LOS DOA estimated using the current estimate of the rover's position and the known LTE eNodeB positions. Figure 2 depicts the block diagram of the LTE-DNN-SAN framework. Further details can be found in Abdallah and Kassas (2020).

In the update step of the EKF, LTE psuedorange measurements are fused in a tightly-coupled manner with the deterministic and the cooperative approaches. For LTE signals that are transmitted from eNodeB j and received by LTE receiver on agent i, the associated pseudorange measurement is denoted as $r_{\text{LTE}_i^j}(k)$. The location of eNodeB j is represented by $\mathbf{p}_{\text{eNodeB}_j}$. The corresponding measurement model, $z_{\text{LTE}_i^j}(k)$, measurement matrix, $\mathbf{H}_{\text{LTE}_i^j}(k)$, and measurement covariance matrix, $\mathbf{R}_{\text{LTE}_i^j}(k)$, are described as follows:

$$z_{\text{LTE}_i^j}(k) = r_{\text{LTE}_i^j}(k),$$

$$\mathbf{H}_{\text{LTE}_i^j}(k) = \begin{bmatrix} \mathbf{0}_{((i-1)\times 30+21)\times 1} \\ \frac{\partial ||\mathbf{p}_{\text{A}_i^r}(k) - \mathbf{p}_{\text{eNodeB}_j}||^\top}{\partial \mathbf{p}_{\text{A}_i^r}(k)} \\ \mathbf{0}_{(6+(N-i)\times 30)\times 1} \\ \mathbf{0}_{((i-1)\times 2)\times 1} \\ 1 \\ \mathbf{0}_{(1+(N-i)\times 2)\times 1} \end{bmatrix}^\top,$$

$$\mathbf{R}_{\text{LTE}_i^j}(k) = \sigma^2_{\text{LTE}_i^j}.$$

Here, $\sigma^2_{\text{LTE}_i^j}$ is an adaptive value based on $c^2 \frac{\alpha}{(C/N_0)_i^j}$, where $(C/N_0)_i^j$ is the signal-to-noise ratios of the pseudorange measurement $r_{\text{LTE}_i^j}(k)$ and α is a tuning parameter that was chosen to be 2.22×10^{-11} (Abdallah and Kassas, 2021). To detect and remove outliers from LTE observables, a rudimentary innovation-based detector is implemented to filter out inconsistent LTE observables Gökalp et al. (2008).

e) Inter-Agent UWB Ranging

The CL approach is realized through inter-agent ranging measurements obtained from UWB sensors attached to the right shoe of each agent. This paper uses $r_{\text{A2A}_i^h}(k)$ to denote the measurements between agent i and agent h. These measurements are classified into LOS and NLOS cases, and only LOS cases are used in the update step of the EKF. The LOS measurements are further processed with bias correction. Assuming that $i < h$, the corresponding inter-agent range measurement model, $z_{\text{A2A}_i^h}(k)$, measurement matrix, $\mathbf{H}_{\text{F2F}_i^h}(k)$, and measurement noise covariance matrices, $\mathbf{R}_{\text{A2A}_i^h}(k)$, are described as follows:

$$z_{\text{A2A}_i^h}(k) = r_{\text{A2A}_i^h}(k),$$

$$\mathbf{H}_{\text{A2A}_i^h}(k) = \begin{bmatrix} \mathbf{0}_{((i-1)\times 30+21)\times 1} \\ \frac{\partial ||\mathbf{p}_{\text{A}_i^r}(k) - \mathbf{p}_{\text{A}_h^r}(k)||^\top}{\partial \mathbf{p}_{\text{A}_i^r}(k)} \\ \mathbf{0}_{(6+(h-i-1)\times 30+21)\times 1} \\ \frac{\partial ||\mathbf{p}_{\text{A}_i^r,k} - \mathbf{p}_{\text{A}_h^r,k}||^\top}{\partial \mathbf{p}_{\text{A}_h^r,k}} \\ \mathbf{0}_{(6+(N-h)\times 30+2N)\times 1} \end{bmatrix}^\top,$$

$$\mathbf{R}_{\text{A2A}_i^h}(k) = \sigma^2_{\text{A2A}_i^h},$$

where $\sigma^2_{\text{A2A}_i^h}$ is the noise variance of the inter-agent range measurements between agent i and agent h.

In the EKF update step, when each of the sensing modalities mentioned previously becomes available, the EKF stacks all available measurements and performs the update step. For example, in a case involving two agents, if measurements of zero-velocity, altimeter, foot-to-foot ranging, inter-agent ranging, and LTE psuedoranges from a nearby LTE tower are all available, the EKF measurement model, $z(k)$, measurement matrix, $\mathbf{H}(k)$, and measurement noise covariance matrix, $\mathbf{R}(k)$, are expressed as follows:

$$z(k) = \begin{bmatrix} \mathbf{z}_{\text{ZUPT}_1^l}(k) \\ \mathbf{z}_{\text{ZUPT}_1^r}(k) \\ \mathbf{z}_{\text{ZUPT}_2^l}(k) \\ \mathbf{z}_{\text{ZUPT}_2^r}(k) \\ z_{\text{ALT}_1^l}(k) \\ z_{\text{ALT}_1^r}(k) \\ z_{\text{ALT}_2^l}(k) \\ z_{\text{ALT}_2^r}(k) \\ z_{\text{F2F}_1}(k) \\ z_{\text{F2F}_2}(k) \\ z_{\text{LTE}_1^1}(k) \\ z_{\text{LTE}_2^1}(k) \\ z_{\text{A2A}_1^2}(k) \end{bmatrix}, \mathbf{H}(k) = \begin{bmatrix} \mathbf{H}_{\text{ZUPT}_1^l}(k) \\ \mathbf{H}_{\text{ZUPT}_1^r}(k) \\ \mathbf{H}_{\text{ZUPT}_2^l}(k) \\ \mathbf{H}_{\text{ZUPT}_2^r}(k) \\ \mathbf{H}_{\text{ALT}_1^l}(k) \\ \mathbf{H}_{\text{ALT}_1^r}(k) \\ \mathbf{H}_{\text{ALT}_2^l}(k) \\ \mathbf{H}_{\text{ALT}_2^r}(k) \\ \mathbf{H}_{\text{F2F}_1}(k) \\ \mathbf{H}_{\text{F2F}_2}(k) \\ \mathbf{H}_{\text{LTE}_1^1}(k) \\ \mathbf{H}_{\text{LTE}_2^1}(k) \\ \mathbf{H}_{\text{A2A}_1^2}(k) \end{bmatrix}, \mathbf{R}(k) = \text{blkdiag}\Bigg(\begin{bmatrix} \mathbf{R}_{\text{ZUPT}_1^l}(k) \\ \mathbf{R}_{\text{ZUPT}_1^r}(k) \\ \mathbf{R}_{\text{ZUPT}_2^l}(k) \\ \mathbf{R}_{\text{ZUPT}_2^r}(k) \\ \mathbf{R}_{\text{ALT}_1^l}(k) \\ \mathbf{R}_{\text{ALT}_1^r}(k) \\ \mathbf{R}_{\text{ALT}_2^l}(k) \\ \mathbf{R}_{\text{ALT}_2^r}(k) \\ \mathbf{R}_{\text{F2F}_1}(k) \\ \mathbf{R}_{\text{F2F}_2}(k) \\ \mathbf{R}_{\text{LTE}_1^1}(k) \\ \mathbf{R}_{\text{LTE}_2^1}(k) \\ \mathbf{R}_{\text{A2A}_1^2}(k) \end{bmatrix}^\top \Bigg)$$

Settings of the noise parameters are determined based on noise characteristics of sensors involved in the implementation.

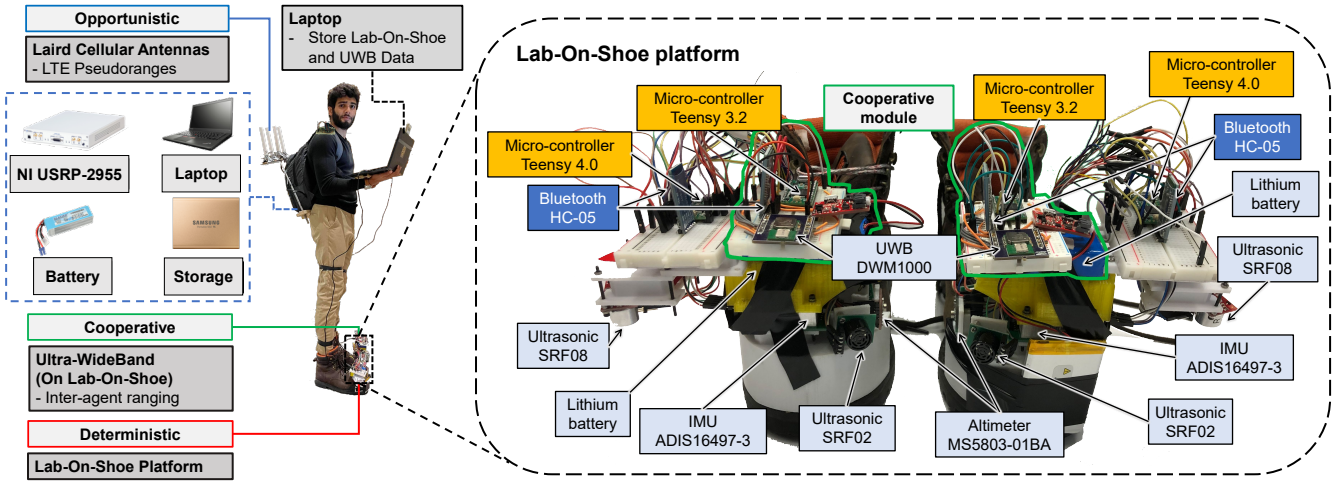

Figure 3: A pedestrian navigation testbed developed to investigate the navigation performance of the PINDOC. The deterministic and cooperative localization approaches were implemented with the Lab-On-Shoe platform, which integrated sensing modalities including IMUs, altimeters, ultrasonic sensors, and UWBs. In this paper, ultrasonic sensors were not used. The opportunistic LTE-based pseudoranges were collected by the Laird cellular Antennas and their corresponding signal processing units. The laptop was used in the experiment for data logging.

III. HARDWARE DESIGN

This section presents a pedestrian navigation testbed designed to evaluate the navigation performance of the PINDOC system. The testbed includes a Lab-On-Shoe platform for the deterministic approach, an LTE receiver for the opportunistic approach, and UWB modules for cooperative localization. Figure 3 and Figure 4 describe the hardware and the firmware of the system, respectively.

1. Lab-On-Shoe Platform: A Flexible Multi-Sensor Navigation Testbed

The Lab-On-Shoe, shown in Figure 3, was developed in Microsystems Lab at the University of California, Irvine, as a reconfigurable multi-sensor pedestrian navigation testbed (S. Askari and C.-S. Jao and Y. Wang and A. M. Shkel, 2019). In this paper, the platform is used to collect all sensor measurements, except for foot-to-foot ranges, that are associated with the deterministic localization. The agent wears the Lab-On-Shoe platform on both left and right feet. Each shoe of the platform includes an Analog Device ADIS16497-3 tactical-grade IMU, an MS5803-01BA barometric altimeter, an SRF08 ultrasonic sensor, and two SRF02 ultrasonic sensors. The barometer has a nominal resolution of 10 cm in vertical displacement measurement, and the ultrasonic sensor has a range resolution of 1 cm. In this paper, the ultrasonic sensors were not used in the experiment discussed in Section IV. A microcontroller Teensy 4.0 is used to implement digital communication protocols, including the Inter-Integrated Circuit (I^2C) and Serial Peripheral Interface (SPI), to collect sensor measurements on the Lab-On-Shoe platform. The sampling rate of IMUs and altimeters are 1000 Hz and 20 Hz, respectively. The collected measurements are transmitted to a laptop with the Universal Asynchronous Receiver-Transmitter (UART) through a USB cable for data logging.

2. LTE Receivers and Processing Modules

In the PINDOC, the opportunistic approach is realized with LTE signals. Each agent in the PINDOC carries a backpack where an LTE receiver is mounted and contains an LTE receiver, a laptop, a battery, and a storage hard drive. The LTE receiver, developed at the Autonomous Systems Perception, Intelligence, & Navigation (ASPIN) Laboratory (Abdallah and Kassas, 2021), is equipped with four consumer-grade cellular omni-directional Laird antennas, and a quad-channel National Instruments (NI) Universal Software Radio Peripheral (USRP)-2955 is used to simultaneously down-mix and synchronously sample LTE signals at 10 Megasamples per second (Msps). The sampled LTE signals are transferred from the USRP-2955 via a PCI Express cable and stored on a laptop for post-processing. The LTE measurements have a sampling rate of 100 Hz.

3. Cooperative UWB modules

One cooperative module, shown in Figure 3, is mounted on each shoe of the Lab-On-Shoe platform. Each of the modules includes a UWB DWM1000, a microcontroller Teensy 3.2, a Bluetooth device HC-05, and a lithium battery (Zhu and Kia, 2019a). The cooperative module was developed in the UC Irvine Kia Cooperative Lab (KCS). The microcontroller operating

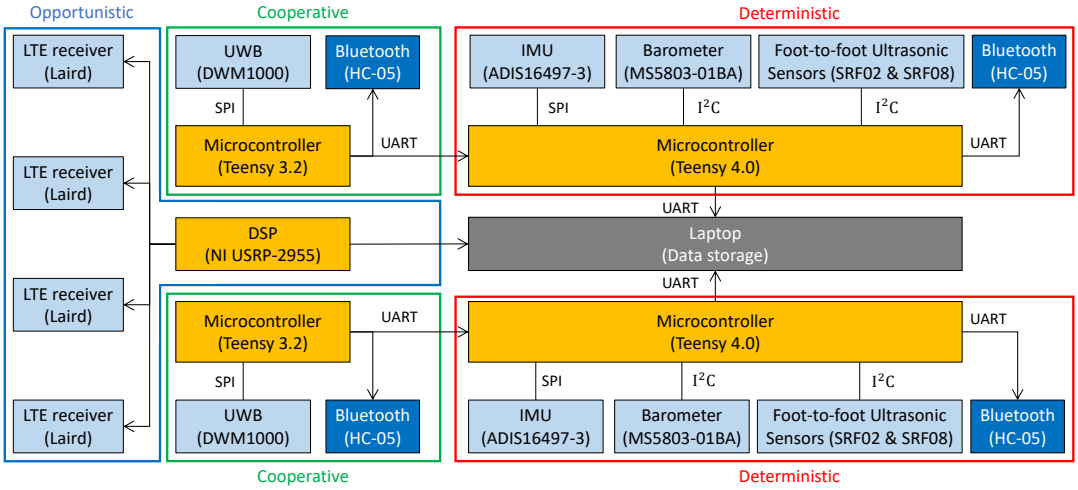

Figure 4: A block diagram illustrating firmware implementation of the pedestrian navigation testbed presented in Figure 3.

at a clock rate of 120 MHz communicates with the UWB via an SPI protocol, and the battery provides a power source for the entire module. The module on the left shoe of an agent is paired up with the modules located on the right foot of all other agents and three pieces of information are obtained: range, power metric (PM), and agent identification (ID). PM is defined as the difference between the total received signal power and the direct-path signal power and is used for LOS/NLOS detection. The range measurements are used for foot-to-foot ranging when obtained from two UWBs mounted on the same agent and for inter-agent ranging when collected from the sensors mounted on two different agents. The collected measurements, including range, PM, and agent ID, are transmitted to nearby Teensy 4.0 on the Lab-On-Shoe platform in UART communication protocol via the Bluetooth transmitter. The sampling rate of the UWB range measurements is 10 Hz.

IV. EXPERIMENTAL VALIDATION

To evaluate the navigation performance of the PINDOC, we conducted two series of multi-agent pedestrian navigation experiments in an indoor environment at the Engineering Gateway Building at the University of California, Irvine. In this section, we describe the experiments, present our experimental results, and discuss the localization performance of the PINDOC.

1. Experiment #1: One Moving Agent, Two Stationary Agents

a) Experiment Description

Three agents were involved in this experiment. Agent No.1, shown in Figure 3, was equipped with the deterministic, opportunistic, and cooperative hardware. Agent No.2 and agent No.3 were both equipped with a set of the cooperative module. Figure 5

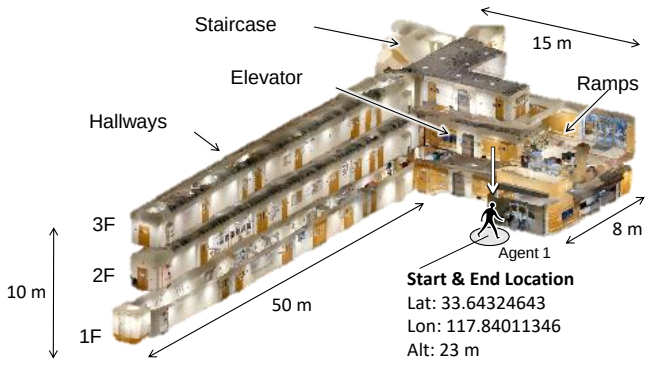

Figure 5: Experimental scenario represented by a point cloud map generated with LiDAR and camera modules installed on iPhone 12 Max Pro. The scenarios included different terrains of flat planes, stairs, ramps, and elevators.

Table 1: LTE ENodeBs' Characteristics

eNodeB	Carrier frequency [MHz]	N_{ID}^{Cell}	Bandwidth [MHz]	Cellular provider
1	2125	223	20	Verizon
2	1955	11	20	AT&T
3	2145	441	20	T-Mobile
4	2112.5	401	20	AT&T

Table 2: Parameters for the EKF used in an experiment discussed in Section IV.1.

Hyper-parameter	Value
σ_{ARW_1}	2.7221×10^{-5}
σ_{VRW_1}	0.0017
σ_{RRW_1}	8.3174×10^{-7}
σ_{AcRW_1}	6.63×10^{-6}
σ_{ZUPT_1}	0.02
σ_{ALT_1}	0.1
σ_{F2F_1}	0.1
σ_{A2A_1}	1
σ_{LTE_1}	$\sqrt{c^2 \frac{2.22\times10^{-11}}{(C/N_0)}}$
$\sigma_{\delta t_{rx_i}}$	1.3×10^{-22}
$\dot{\sigma}_{\delta t_{rx_i}}$	7.8957×10^{-25}

presents a point cloud dataset representing the experimental scenario. The point cloud data was collected with a LiDAR module and cameras installed in an iPhone 12 Max. At the beginning of the experiment, agent No.1 stood outside of the first floor of the building for one minute to initialize the system. The GNSS and the altimeter mounted on agent No.1 obtained the initial global position in latitude, longitude, and altitude during this period. The LTE receiver was initialized and started to track signals transmitted from four eNodeBs. The eNodeBs' characteristics are summarized in Table 1. In the initialization process, we calibrated accelerometer and gyroscope turn-on biases of the IMUs with the approaches described in (Jao et al., 2022b). Noise parameters used in the EKF for PINDOC are listed in Table 2.

After initialization, agent No.1 walked inside the building with a trajectory represented by the blue and red curves in Figure 6. The navigation scenarios included flat planes, stairs, ramps, and elevators. The length of the path was around 600 meters, and the duration was approximately 14 minutes. During the experiment, agent No.1 passed by the checkpoints marked with the green triangles in Figure 6. The locations of the checkpoints were pre-survey with an industrial ruler. The experiment was recorded using a smartphone camera, and the timestamps at which the agent passed through each checkpoint were visually determined from the video. During the entire experiment, agent No.2 and agent No.3 remained stationary at the locations marked by the red and blue star markers in Figure 6. The UWB sensors mounted on the right shoe of agent No.1 had an LOS connection with agent No.2 from 250 s to 310 s and with agent No.3 from 430 s to 485 s. Communication was lost in other periods of time because the UWB modules were too far apart and due to obstacles between the UWB modules. The measurements collected in this experiment indicate that the maximum communication range for the UWBs was around 30 m when there was a clear path for signals to be transmitted.

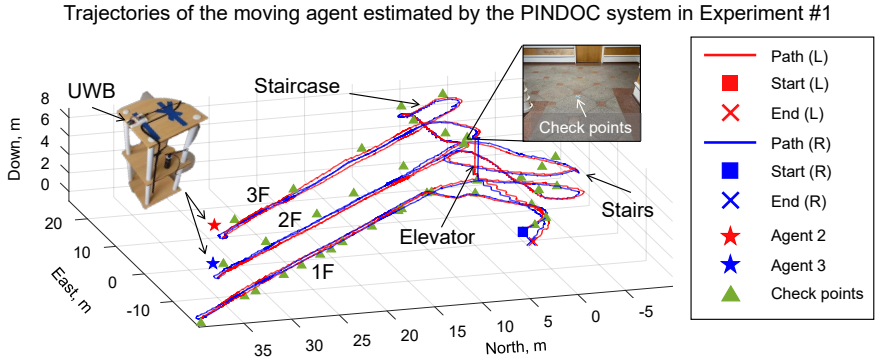

Figure 6: The blue and red curves represent the navigation trajectories of the two feet of agent No.1 estimated by the PINDOC implementing the ZUPT-aided INS augmented by altimeters, foot-to-foot ranging, and inter-agent ranging measurements in the experiment discussed in Section IV.1. The blue star and the red star marked the locations of stationary agent No.2 and agent No.3 in the navigation frame. The green triangles mark checkpoints that were used to evaluate the in-trajectory localization accuracy of the navigation solutions.

Table 3: Navigation error of the PINDOC implemented in different configurations in an experiment discussed in Section IV.1.

Config.	INS Aiding Method						Processing	RMSE [m]	2D	⊥	SD [m]	Max	Final
	ZUPT	ALT	F2F	A2	A3	LTE	**Time** (s)		**RMSE** [m]	**RMSE** [m]		**Error** [m]	**Error** [m]
G	✓	✓	✓	✓	✓	✓	231.7	0.93	0.69	0.62	0.44	2.23	1.28
F	✓	✓	✓	✓	✓		211.6	0.93	0.69	0.62	0.44	2.23	1.32
D	✓	✓	✓	✓			211.0	0.94	0.71	0.62	0.43	2.23	1.32
E	✓	✓	✓		✓		210.9	0.95	0.72	0.62	0.46	2.23	1.68
I	✓	✓	✓			✓	227.0	0.96	0.74	0.62	0.45	2.23	1.64
C	✓	✓	✓				210.3	0.97	0.75	0.62	0.46	2.23	1.76
J	✓	✓				✓	234.0	1.07	0.87	0.62	0.48	2.44	1.51
B	✓	✓					207.4	1.64	1.52	0.59	0.75	2.9	2.55
K		✓				✓	227.9	1.97	1.65	0.67	0.88	7.74	3.2
H	✓					✓	222.0	2.48	0.90	2.32	1.87	10.02	10.02
A	✓						191.5	2.53	0.49	2.48	1.9	10.3	10.3

b) Performance Metrics

We considered seven performance metrics in this experiment, including one computational complexity metric and six different accuracy metrics, to evaluate the navigation performance of the PINDOC. Table 3 lists these metrics, which are processing time, position Root-Mean-Square Error (RMSE), two-dimensional (2D) RMSE, vertical ($\perp$) RMSE, position error Standard Deviation (SD), maximum displacement error, and final position error. In this paper, the processing time is used to evaluate the computational complexity of a localization solution. The processing time was calculated based on the amount of time for the 2021a MATLAB program, operating on a laptop with an AMD Ryzen 9 5900HS Central Processing Unit (CPU) running at a clock rate of around 4 GHz, to compute a navigation solution based on collected sensor measurements.

The six accuracy metrics were chosen so that the navigation performance of the PINDOC can be conveniently compared with the localization accuracy of other indoor navigation systems discussed in the literature. Among these six metrics, RMSE is often used to evaluate an estimated localization solution when reference trajectories along the three dimensions are available. 2D RMSE and $\perp$ RMSE are used as benchmarks when estimated positioning solutions emphasize accuracy in the horizontal and vertical directions, respectively. Position error SD is used to quantify variations of displacement error. Maximum displacement error is used to investigate the worst-case scenarios of an estimated position. Finally, final position error is often used to evaluate dead-reckoning systems, which have localization errors accumulating with time, in navigation experiments where obtaining reference trajectories is challenging. For example, when evaluating pedestrian navigation systems using foot-mounted IMUs, navigation experiments could involve trajectories that cover large indoor areas, on the order of 50-100 m, and include a combination of complex terrains, such as flat planes, stairs, ramps, ladders, and elevators (Abdallah et al., 2022). In such environments, it can be very expensive to deploy a high-precision position reference system like the Opti-Track (Yuan et al., 2013) or the Vicon (Angermann et al., 2010), and therefore, final position errors are used in these scenarios.

c) Experimental Results

We compared the navigation performance for agent No.1 using the PINDOC implemented in different configurations. Different configurations of the PINDOC use the ZUPT-aided INS, augmented by different combinations of various sensing modalities, namely altimeter (ALT), foot-to-foot ranging (F2F), inter-agent ranging with agent No.2 (A2) and agent No.3 (A3), and cellular LTE pseudorange measurements.

We used the seven performance metrics discussed in Section IV.1 b) to quantify the localization error at each checkpoint for each navigation solution. Table 3 summarizes the performance of the navigation solutions using the PINDOC implemented in different configurations. The accuracy values presented in Table 3 were calculated based on the 38 checkpoints marked by the green triangles in Figure 6. For the configurations where foot-to-foot ranging measurements were not involved, the accuracy metrics were calculated based on solutions of agent No.1's right foot as inter-agent range measurements were collected with the UWB module mounted on the right foot. The top item Table 3, which is PINDOC with configuration G that uses ZUPT-aided INS augmented by ALT, F2F, A2, A3, and LTE had the smallest RMSE of 0.93 m. The bottom item in Table 3, which is PINDOC with configuration A, had the largest RMSE of 2.53 m.

We concluded six remarks from Table 3.

- It could be observed that enhancing the ZUPT-aided INS with more aiding methods led to better navigation accuracy, however, with a trade-off of increasing computational complexity. Configuration G that uses the INS aided by the ZUPT algorithm, altimeter, foot-to-foot ranging measurements, the inter-agent range measurements from the other two agents, and LTE pseudorange measurements had the smallest displacement error.

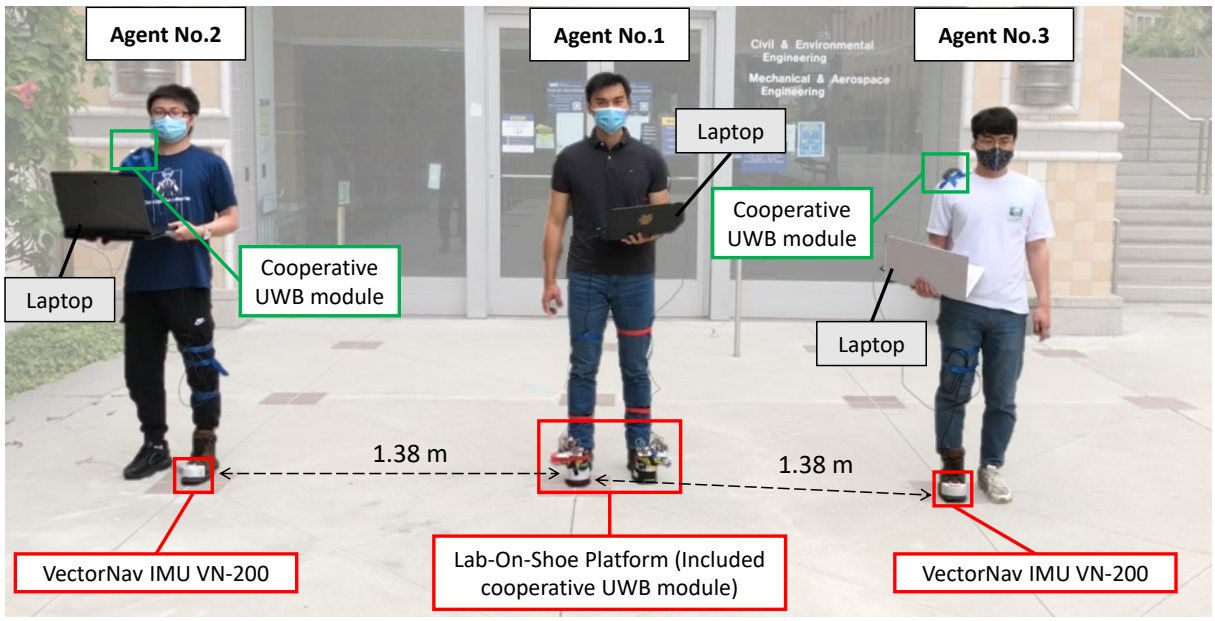

Figure 7: Experimental setup of the experiment discussed in Section IV.2.

- We could observe that the maximum position errors did not always occur at the end of the experiment. This could be because, for dead reckoning systems, estimation errors on trajectory length get canceled out at return-to-home or loop-closure positions.
- In the configurations involving the LTE module, an innovation-based outlier detection module, as discussed in Section II.3 d), was used to produce the opportunistic navigation solutions. The outlier detection module detected if the LTE signal had large biases caused by the multi-path effect. In the case of a positive detection, the LTE psuedorange measurement was not used to augment the navigation solutions. It is worth mentioning that, in the experiment, we observed that the outlier detection module indicated several positive detections, and therefore, not all the LTE signals collected during the experiment were used in configuration G, H, I, and J. Nevertheless, when the outlier detection module showed negative detections, the opportunistic solution provided compensation for absolute position errors, increasing navigation accuracy.
- Configuration D and configuration E used deterministic solutions enhanced by inter-agent measurements from only one agent, but the former configuration had a smaller final displacement error. We considered the difference as a result of the experimental setup that agent No.1 first passed by agent No.3 and then agent No.2. This setup led to an advantage of configuration D in that the position estimates were corrected by the stationary agent at a later time, and therefore, the final position estimated by configuration D had a smaller error than configuration E.
- In the cases where altimeter measurements were not used, which are configurations A and H, the final position errors are much larger than in the other configurations. For configuration A, the final error is larger because when operating in the moving elevator, the stance phase detector used in the ZUPT algorithm would indicate that it is the stance phase and correct the velocity to zero, while in reality, the altitude of the agent was changing. In configuration H, we could see that augmenting the ZUPT-aided INS with LTE measurements could reduce the error. However, the horizontal distance between the receiver is significantly larger than the altitude of the LTE towers. As such, the agent's cellular-based navigation solution Vertical Dilution Of Precision (VDOP) will be large. Yet, LTE reduced the vertical errors slightly compared to standalone ZUPT.
- In the PINDOC, aiding from LTE pseudorange measurements aims to bound absolute position error propagation. In the presented experiment with a duration of 14 min and a trajectory length of 600 m, the position errors in systems using only the deterministic and cooperative approaches have not grown to large values. Therefore, the correction of errors provided by LTE signals was not significant. However, it is expected that in navigation experiments with a longer duration, the LTE module will play a significant role in bounding the position error growth of PINDOC and improving navigation accuracy.

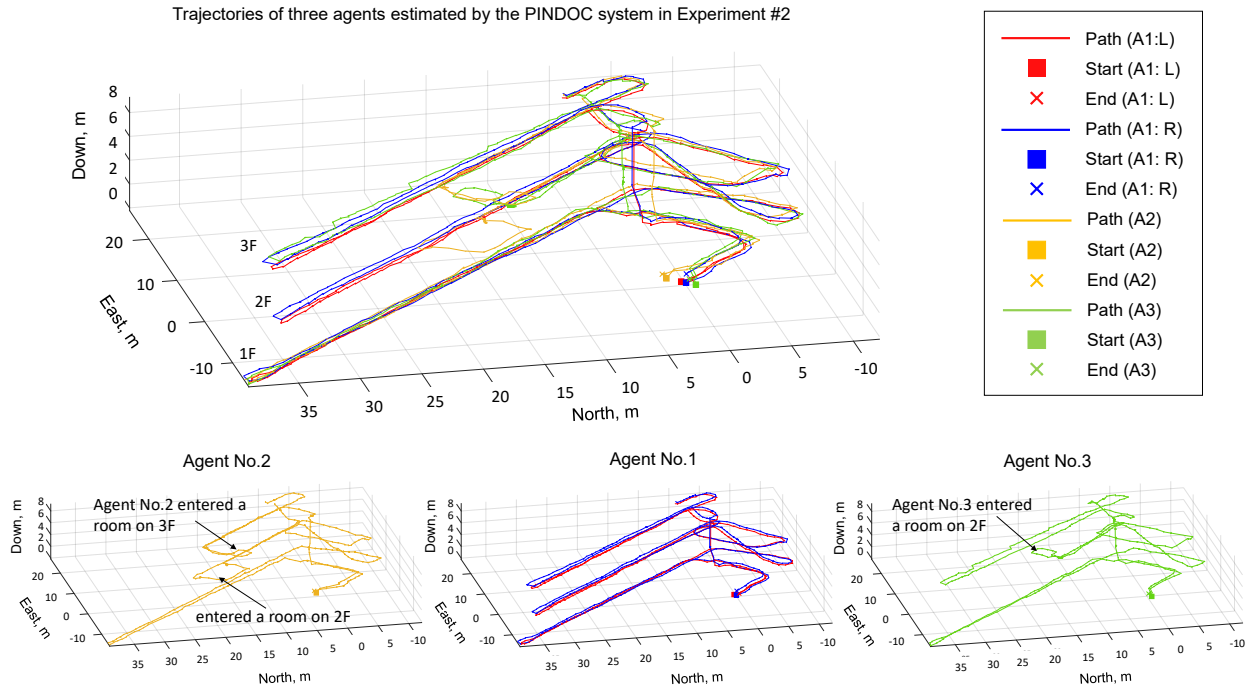

Figure 8: The top plot shows the navigation solutions of the three agents produced by the PINDOC system in the experiment discussed in Section IV.2. The bottom three plots separately present the same navigation solution of each agent. Agent No.1's trajectories were generated with the ZUPT-aided INS augmented with altimeter measurements, foot-to-foot ranging, and inter-agent ranging measurements. Agent No.2 and agent No.3's trajectories were generated with the ZUPT-aided INS augmented with altimeter measurements, and inter-agent ranging measurements.

2. Experiment #2: Three Moving Agents

a) Experiment Description

The second series of experiments involved three agents, all moving in the indoor environment shown in Figure 5. The experimental setup is shown in Figure 7. Agent No.1 was equipped with the Lab-On-Shoe platform integrated with the cooperative UWB modules discussed in Section III. Agent No.2 in Figure 7 mounted a VectorNav VN-200 IMU on the left foot and attached a cooperative UWB module at the right shoulder. The position of the UWB module was assumed to be 1.4 m above the foot-mounted IMU. Agent No.3 in Figure 7 mounted another VectorNav VN-200 IMU on the right foot and attached another cooperative UWB module at the right shoulder. The position of the UWB module on agent No.3 was assumed to be 1.3 m above the foot-mounted IMU. Both VN-200 IMUs were configured to collect IMU measurements at a sampling rate of 800 Hz and altimeter measurements at a sampling rate of 10 Hz. The UWB modules attached to agent No.2 and agent No.3 were not connected with each other and were both programmed to be paired with the cooperative UWB module integrated on the right shoe of the Lab-On-Shoe platform used by agent No.1. In Figure 7, the location of agent No.1's right foot was considered as the origin of the local coordinate frame, which had the same global coordinates as the starting position shown in Figure 5. The starting positions of the other two agents were 1.38 m apart from the origin, as shown in Figure 7.

At the beginning of the experiment, the three agents stood stationary at their starting positions for 15 seconds. During this period, all IMUs were calibrated. Then, agent No.3 first walked inside the building, followed by agent No.2 and then agent No.3. Figure 8 presents the trajectories of the three agents. The duration of the experiment was around 12.5 minutes and the lengths of the trajectories corresponding to agent No.1, agent No.2, and agent No.3 were around 600 m, 540 m, and 550 m, respectively. The three agents traveled on different terrains, including flat planes, stairs, slopes, and elevators. From timestamps of 420 s to 443 s and from 568 s to 596 s, agent No. 2 entered office spaces and did not have LOS UWB range measurements with agent No.1. From timestamps of 346 s to 422 s, agent No.3 entered a laboratory space and did not have LOS UWB range measurements with agent No.1. At the end of the experiment, the three agents returned to their starting positions.

Table 4: Navigation errors of the PINDOC implemented in different configurations in an experiment discussed Section IV.2

Agent	INS Aiding Method				Final
	ZUPT	ALT	F2F	CL	Error [m]
No.1	✓	✓	✓	✓	0.35
	✓	✓	✓		0.44
	✓	✓			0.84
	✓				10.27
No.2	✓	✓		✓	0.82
	✓	✓			4.25
	✓				13.41
No.3	✓	✓		✓	1.15
	✓	✓			4.38
	✓				15.83

b) Experimental Results

In this experiment, we used the loop-closure error, described in Section IV.1 b), as the accuracy metric to compare the PINDOC system implemented in different configurations. Four different PINDOC configurations involving ZUPT, ALT, F2F, and CL, were used to produce navigation solutions for agent No.1, and three different PINDOC configurations involving ZUPT, ALT, and CL, were used to estimate navigation solutions for agent No.2 and agent No.3. In the case of CL, inter-agent range measurements between agent No.1 and agent No.2 as well as the range measurements between agent No.1 and agent No.3 were used. Table 4 presents the navigation accuracy of the different configurations for different agents.

Three remarks could be made based on the experimental results shown in Table 4.

- The navigation solutions of the three agents based on standalone ZUPT-aided INS had the largest errors because the stance phase detector used in the ZUPT algorithm indicated stationary phases when the agents were inside a moving elevator, leading to falsely updating the velocity estimate to zero. The errors introduced by the elevator were also discussed previously in Section IV.1 c). When altimeters were used to enhance the navigation solutions, the errors associated with the three agents were reduced.
- when inter-agent range measurements were used, the errors of agent No. 2 and agent No.3 were greatly reduced while the error of agent No.1 had only a marginal improvement. This phenomenon was because, as compared to the IMUs on the Lab-On-Shoe platform, the VectorNav IMUs mounted on agent No.2 and agent No.3 had higher noise levels and biases, leading to position uncertainties growing faster than the uncertainties of agent No.1. As a result, inter-agent range measurements had larger impacts on positions of agent No.2 and agent No.3 in this experiment than those of agent No.1.
- Among all the PINDOC implementations used in the experiment, the implementation using ZUPT-aided INS augmented with altimeter, foot-to-foot ranging, and inter-agent ranging had the smallest loop-closure errors of 0.35 m for agent No.1, 0.82 m for agent No.2, and 1.15 m for agent No.3. The trajectories of the three agents estimated by the later PINDOC implementation are presented in Figure 8.

V. CONCLUSION

This paper experimentally evaluated the navigation performance of the PINDOC system, which integrates the deterministic, the opportunistic, and the cooperative localization approaches. The deterministic approach uses a ZUPT-aided INS augmented with measurements of altimeters and foot-to-foot ranging. The opportunistic navigation provides global position compensation to the deterministic approach based on LTE psuedoranges. The cooperative localization is realized based on UWB-based inter-agent range measurements. We reported two series of indoor pedestrian navigation experiments involving three agents to investigate the navigation performance of the PINDOC. In the first series of experiments, one agent traveled in an indoor environment that included terrains of flat planes, stairs, slopes, and elevators, for 600 m in 14 minutes, and the other two agents remained stationary throughout the entire experiment. We compared a variety of PINDOC configurations using different combinations of the deterministic, the opportunistic, and the cooperative components. Among all the configurations, the navigation solution using the ZUPT-aided INS enhanced with altimeters, foot-to-foot ranging, UWB-based inter-agent ranging, and LTE psuedoranges had the highest navigation accuracy in this experiment, with a position RMSE of 0.93 m and a position error SD of 0.44 m. The second series of experiments involved three agents navigating in the same indoor environment along close-loop trajectories for a duration of 12.5 minutes. We compared the localization accuracy of the PINDOC configurations using combinations of the

deterministic and the cooperative approaches in this experiment. The experimental results showed that the lowest loop-closure errors were achieved with the localization solution using the ZUPT-aided INS enhanced with altimeters, foot-to-foot ranging, and UWB-based inter-agent ranging, and the errors for the three agents were 0.35 m, 0.82 m, and 1.15 m, respectively.

ACKNOWLEDGEMENTS

The authors would like to thank Jeb Benson, Former Technical Program Manager at NIST Public Safety Communication Research (PSCR), and Joseph Grasso, Portfolio Lead at PSCR Location-Based Services (LBS), for useful discussions. The content of this article is solely the responsibility of the authors and does not necessarily represent the official views of NIST.

REFERENCES

Abdallah, A., Jao, C., Kassas, Z., and Shkel, A. (2022). A pedestrian indoor navigation system using deep-learning-aided cellular signals and ZUPT-aided foot-mounted IMUs. *IEEE Sensors Journal*, 22(6):5188–5198.

Abdallah, A. and Kassas, Z. (2020). Deep learning-aided spatial discrimination for multipath mitigation. In *Proceedings of IEEE/ION Position, Location, and Navigation Symposium*, pages 1324–1335.

Abdallah, A. and Kassas, Z. (2021). Multipath mitigation via synthetic aperture beamforming for indoor and deep urban navigation. *IEEE Transactions on Vehicular Technology*, 70(9):8838–8853.

Abdallah, A., Khalife, J., and Kassas, Z. (2021). Experimental characterization of received 5G signals carrier-to-noise ratio in indoor and urban environments. In *Proceedings of IEEE Vehicular Technology Conference*, pages 1–5.

Angermann, M., Robertson, P., Kemptner, T., and Khider, M. (2010). A high precision reference data set for pedestrian navigation using foot-mounted inertial sensors. In *Proceedings of IEEE International Conference on Indoor Positioning and Indoor Navigation*, pages 1–6.

Chen, C., Jao, C., Shkel, A., , and Kia., S. (2022). UWB sensor placement for foot-to-foot ranging in dual-foot mounted ZUPT-aided INS. *IEEE Sensors Letters*, 6(2):1–4.

de Ponte Müller, F. (2017). Survey on ranging sensors and cooperative techniques for relative positioning of vehicles. *Sensors*, 17(2):271.

Dun, H., Tiberius, C., and Janssen, G. (2020). Positioning in a multipath channel using OFDM signals with carrier phase tracking. *IEEE Access*, 8:13011–13028.

Ferreira, A., Fernandes, D., Catarino, A., and Monteiro, J. (2017). Localization and positioning systems for emergency responders: A survey. *IEEE Communications Surveys & Tutorials*, 19(4):2836–2870.

Foxlin, E. (2005). Pedestrian tracking with shoe-mounted inertial sensors. *IEEE Computer graphics and applications*, 25(6):38–46.

Gökalp, E., Güngör, O., and Boz, Y. (2008). Evaluation of different outlier detection methods for GPS networks. *Sensors*, 8(11):7344–7358.

Ikhtiari, N. (2019). Navigation in GNSS denied environments using software defined radios and LTE signals of opportunities. Master's thesis, University of Canterbury, Christchurch, New Zealand.

Jao, C., Abdallah, A., Chen, C., Seo, M., Kia, S., Kassas, Z., and Shkel, A. (2022a). PINDOC: Pedestrian indoor navigation system integrating deterministic, opportunistic, and cooperative functionalities. *IEEE Sensors Journal*, 22(14):14424–14435.

Jao, C., Parrish, A., and Shkel, A. (2021). "sugar-cube" PLT: A real-time pedestrian localization testbed utilizing foot-mounted IMU/barometer/ultrasonic sensors. In *Proceedings of IEEE Sensors Conference*, pages 1–4.

Jao, C. and Shkel, A. (2021a). A reconstruction filter for saturated accelerometer signals due to insufficient FSR in foot-mounted inertial navigation system. *IEEE Sensors Journal*, 22(1):695–706.

Jao, C. and Shkel, A. (2021b). ZUPT-aided ins bypassing stance phase detection by using foot-instability-based adaptive covariance. *IEEE Sensors Journal*, 21(21):24338–24348.

Jao, C., Wang, D., Parrish, A., and Shkel, A. (2022b). A neural network approach to mitigate thermal-induced errors in ZUPT-aided INS. In *Proceedings of IEEE International Symposium on Inertial Sensors and Systems*, pages 1–4.

Jao, C., Wang, W., Askari, S., and Shkel, A. (2020a). A closed-form analytical estimation of vertical displacement error in pedestrian navigation. In *Proceedings of IEEE/ION Position, Location and Navigation Symposium*, pages 793–797.

Jao, C., Wang, Y., Lin, Y., and Shkel, A. (2020b). A hybrid barometric/ultrasonic altimeter for aiding ZUPT-based inertial pedestrian navigation systems. In *Proceedings of ION GNSS+ Conference*, pages 2500–2517.

Jao, C., Wang, Y., and Shkel, A. (2020c). Pedestrian inertial navigation system augmented by vision-based foot-to-foot relative position measurements. In *Proceeding IEEE/ION Position, Location and Navigation Symposium*, pages 900–907.

Jao, C., Wang, Y., and Shkel, A. (2020d). A zero velocity detector for foot-mounted inertial navigation systems aided by downward-facing range sensor. In *Proceedings of IEEE Sensors Conference*, pages 1–4.

Jao, C.-S., Stewart, K., Conradt, J., Neftci, E., and Shkel, A. (2020e). Zero velocity detector for foot-mounted inertial navigation system assisted by a dynamic vision sensor. In *DGON Inertial Sensors and Systems (ISS)*. Sep. 15-16, Virtual Conference.

Kassas, Z. (2021). Position, navigation, and timing technologies in the 21st century. volume 2, chapter 38: Navigation with Cellular Signals of Opportunity, pages 1171–1223. Wiley-IEEE.

Kassas, Z. and Humphreys, T. (2014). Observability analysis of collaborative opportunistic navigation with pseudorange measurements. *IEEE Transactions on Intelligent Transportation Systems*, 15(1):260–273.

Kassas, Z., Khalife, J., Shamaei, K., and Morales, J. (2017a). I hear, therefore I know where I am: Compensating for GNSS limitations with cellular signals. *IEEE Signal Processing Magazine*, pages 111–124.

Kassas, Z., Morales, J., Shamaei, K., and Khalife, J. (2017b). LTE steers UAV. *GPS World Magazine*, 28(4):18–25.

Kleinman, R. and Merkel, C. (2020). Digital contact tracing for COVID-19. *Canadian Medical Association Journal*, 192(24):E653–E656.

Kumar, G., Patil, A., Patil, R., Park, S., and Chai, Y. (2017). A LiDAR and IMU integrated indoor navigation system for UAVs and its application in real-time pipeline classification. *Sensors*, 17(6):1268–1291.

Laverne, M., George, M., Lord, D., Kelly, A., and Mukherjee, T. (2011). Experimental validation of foot-to-foot range measurements in pedestrian tracking. In *Proceedings of ION GNSS Conference*, pages 1386–1393.

Lemaire, T., Berger, C., Jung, I.-K., and Lacroix, S. (2007). Vision-based SLAM: Stereo and monocular approaches. *International Journal of Computer Vision*, 74(3):343–364.

Ma, M., Song, Q., Gu, Y., Li, Y., and Zhou, Z. (2018). An adaptive zero velocity detection algorithm based on multi-sensor fusion for a pedestrian navigation system. *Sensors*, 18(10):3261–3276.

Maaref, M. and Kassas, Z. (2022). Autonomous integrity monitoring for vehicular navigation with cellular signals of opportunity and an IMU. *IEEE Transactions on Intelligent Transportation Systems*, 23(6):5586–5601.

Minetto, A. and Dovis, F. (2019). On the information carried by correlated collaborative ranging measurements for hybrid positioning. *IEEE Transactions on Vehicular Technology*, 69(2):1419–1427.

Morales, J. and Kassas, Z. (2018). Optimal collaborative mapping of terrestrial transmitters: receiver placement and performance characterization. *IEEE Transactions on Aerospace and Electronic Systems*, 54(2):992–1007.

Morales, J. and Kassas, Z. (2019). Stochastic observability and uncertainty characterization in simultaneous receiver and transmitter localization. *IEEE Transactions on Aerospace and Electronic Systems*, 55(2):1021–1031.

Morales, J., Khalife, J., and Kassas, Z. (2022). Information fusion strategies for collaborative inertial radio SLAM. *IEEE Transactions on Intelligent Transportation Systems*, 23(8):12935–12952.

Nilsson, J., Skog, I., and Händel, P. (2012). A note on the limitations of ZUPTs and the implications on sensor error modeling. In *Proceedings of International Conference on Indoor Positioning and Indoor Navigation*, pages 1–4.

Nilsson, J.-O., Gupta, A. K., and Händel, P. (2014). Foot-mounted inertial navigation made easy. In *Proceedings of International Conference on Indoor Positioning and Indoor Navigation*, pages 24–29.

Nilsson, J.-O., Zachariah, D., Skog, I., and Händel, P. (2013). Cooperative localization by dual foot-mounted inertial sensors and inter-agent ranging. *EURASIP Journal on Advances in Signal Processing*, 2013(1):1–17.

Norrdine, A., Kasmi, Z., and Blankenbach, J. (2016). Step detection for ZUPT-aided inertial pedestrian navigation system using foot-mounted permanent magnet. *IEEE Sensors Journal*, 16(17):6766–6773.

Pan, M., Liu, P., Liu, S., Qi, W., Huang, Y., You, X., Jia, X., and Li, X. (2022). Efficient joint DOA and TOA estimation for indoor positioning with 5G picocell base stations. *IEEE Transactions on Instrumentation and Measurement*, 71:1–19.

Renaudin, V., Ortiz, M., Perul, J., Torres-Sospedra, J., Jiménez, A., Pérez-Navarro, A., Mendoza-Silva, G., Seco, F., Landau, Y., Marbel, R., et al. (2019). Evaluating indoor positioning systems in a shopping mall: The lessons learned from the IPIN 2018 competition. *IEEE Access*, 7:148594–148628.

Ruiz, A. and Granja, F. (2017). Comparing ubisense, bespoon, and decawave UWB location systems: Indoor performance analysis. *IEEE Transactions on instrumentation and Measurement*, 66(8):2106–2117.

S. Askari and C.-S. Jao and Y. Wang and A. M. Shkel (2019). A laboratory testbed for self-contained navigation. In *Proceedings of IEEE International Symposium on Inertial Sensors and Systems*, pages 1–2.

Sevrin, L., Noury, N., Abouchi, N., Jumel, F., Massot, B., and Saraydaryan, J. (2015). Characterization of a multi-user indoor positioning system based on low cost depth vision (Kinect) for monitoring human activity in a smart home. In *Proceedings of Annual International Conference of the IEEE Engineering in Medicine and Biology Society*, pages 5003–5007.

Shamaei, K. and Kassas, Z. (2018). LTE receiver design and multipath analysis for navigation in urban environments. *NAVIGATION, Journal of the Institute of Navigation*, 65(4):655–675.

Shkel, A. and Wang, Y. (2021). *Pedestrian Inertial Navigation with Self-Contained Aiding*. IEEE Press Series on Sensors. Wiley.

Shu, Y., Huang, Y., Zhang, J., Coué, P., Cheng, P., Chen, J., and Shin, K. (2015). Gradient-based fingerprinting for indoor localization and tracking. *IEEE Transactions on Industrial Electronics*, 63(4):2424–2433.

Skog, I., Handel, P., Nilsson, J., and Rantakokko, J. (2010). Zero-velocity detection—an algorithm evaluation. *IEEE Transactions On Biomedical Engineering*, 57(11):2657–2666.

Souli, N., Makrigiorgis, R., Kolios, P., and Ellinas, G. (2021a). Cooperative relative positioning using signals of opportunity and inertial and visual modalities. In *Proceedings IEEE Vehicular Technology Conference*, pages 1–7.

Souli, N., Makrigiorgis, R., Kolios, P., and Ellinas, G. (2021b). Real-time relative positioning system implementation employing signals of opportunity, inertial, and optical flow modalities. In *Proceedings of International Conference on Unmanned Aircraft Systems*, pages 229–236.

Strandjord, K., Morton, Y., and Wang, P. (2021). Evaluating the urban signal environment for GNSS and LTE signals. In *Proceedings of ION GNSS+ Conference*, pages 2166–2182.

Tejesh, B. and Neeraja, S. (2018). Warehouse inventory management system using IoT and open source framework. *Alexandria Engineering Journal*, 57(4):3817–3823.

Titterton, D. and Weston, J. (2004). *Strapdown inertial navigation technology*, volume 17. IET, London, United Kingdom, second edition.

Wahlström, J. and Skog, I. (2020). Fifteen years of progress at zero velocity: A review. *IEEE Sensors Journal*, 21(2):1139–1151.

Wang, P. and Morton, Y. (2020). Multipath estimating delay lock loop for LTE signal TOA estimation in indoor and urban environments. *IEEE Transactions on Wireless Communications*, 19(8):5518–5530.

Wang, P., Wang, Y., and Morton, J. (2022). Signal tracking algorithm with adaptive multipath mitigation and experimental results for LTE positioning receivers in urban environments. *IEEE Transactions on Aerospace and Electronic Systems*, 58(4):2779–2795.

Wang, Q., Guo, Z., Sun, Z., Cui, X., and Liu, K. (2018a). Research on the forward and reverse calculation based on the adaptive zero-velocity interval adjustment for the foot-mounted inertial pedestrian-positioning system. *Sensors*, 18(5):1642–1657.

Wang, Y., Askari, S., Jao, C.-S., and Shkel, A. M. (2019). Directional ranging for enhanced performance of aided pedestrian inertial navigation. In *Proceedings of IEEE International Symposium on Inertial Sensors and Systems*, pages 1–2.

Wang, Y., Chernyshoff, A., and Shkel, A. M. (2018b). Error analysis of ZUPT-aided pedestrian inertial navigation. In *Proceesings of International Conference on Indoor Positioning and Indoor Navigation*, pages 206–212.

Wang, Y., Jao, C.-S., and Shkel, A. (2021). Scenario-dependent ZUPT-aided pedestrian inertial navigation with sensor fusion. *Journal of Gyroscopy and Navigation*, 12(1):1–16.

Wang, Y., Lin, Y.-W., Askari, S., Jao, C.-S., and Shkel, A. M. (2020). Compensation of systematic errors in ZUPT-aided pedestrian inertial navigation. In *Proceedings of IEEE/ION Position, Location and Navigation Symposium*, pages 1452–1456.

Whiton, R., Chen, J., Johansson, T., and Tufvesson, F. (2022). Urban navigation with LTE using a large antenna array and machine learning. In *Proceedings of IEEE Vehicular Technology Conference*, pages 1–5.

Xu, L. and Rife, J. (2020). Modeling multipath effects on frequency locked loops. In *Proceedings of ION International Technical Meeting*, pages 698–712.

Yang, C., Arizabaleta-Diez, M., Weitkemper, P., and Pany, T. (2022). An experimental analysis of cyclic and reference signals of 4g LTE for TOA estimation and positioning in mobile fading environments. *IEEE Aerospace and Electronic Systems Magazine*, 37(9):16–41.

Yuan, Q., Chen, I.-M., and Caus, A. (2013). Human velocity tracking and localization using 3 imu sensors. In *Proceedings of IEEE Conference on Robotics, Automation and Mechatronics (RAM)*, pages 25–30.

Zhu, J. and Kia, S. (2018). A loosely coupled cooperative localization augmentation to improve human geolocation in indoor environments. In *Proceedings of International Conference on Indoor Positioning and Indoor Navigation*, pages 206–212.

Zhu, J. and Kia, S. (2019a). Bias compensation for UWB ranging for pedestrian geolocation applications. *IEEE Sensors Letters*, 3(9):1–4.

Zhu, J. and Kia, S. (2019b). Cooperative localization under limited connectivity. *IEEE Transactions on Robotics*, 35(6):1523–1530.

Zhu, J. and Kia, S. (2020). An UWB-based communication protocol design for an infrastructure-free cooperative navigation. In *Proceedings of IEEE/ION Position, Location and Navigation Symposium*, pages 360–366.

Zhu, J. and Kia, S. (2021). Decentralized cooperative localization with LoS and NLoS UWB inter-agent ranging. *IEEE Sensors Journal*, pages 5447–5456.

Zhuang, Y., Yang, J., Li, Y., Qi, L., and El-Sheimy, N. (2016). Smartphone-based indoor localization with bluetooth low energy beacons. *Sensors*, 16(5):596–615.